Supporting Information: Complex-birefringent dielectric metasurfaces for arbitrary polarization-pair transformations

Shaun Lung,[1,*] Kai Wang,[1,2] Khosro Zangeneh Kamali,[3] Jihua Zhang,[1] Mohsen Rahmani,[3,4] Dragomir N. Neshev,[3] and Andrey A. Sukhorukov[1,†]

[1]*ARC Centre of Excellence for Transformative Meta-Optical Systems (TMOS), Nonlinear Physics Centre, Research School of Physics, The Australian National University, Canberra, ACT 2601, Australia*

[2]*Ginzton Laboratory and Department of Electrical Engineering, Stanford University, Stanford, CA 94305, USA*

[3]*ARC Centre of Excellence for Transformative Meta-Optical Systems (TMOS), Department of Electronic Materials Engineering, Research School of Physics, The Australian National University, Canberra, ACT 2601, Australia*

[4]*Advanced Optics and Photonics Laboratory, Department of Engineering, School of Science and Technology, Nottingham Trent University, Nottingham, NG11 8NS, UK*

This Supporting Information contains 10 pages, 5 sections, 3 figures, which provide extra details on the theoretical and experimental aspects of our work.

* shaun.lung@anu.edu.au

† andrey.sukhorukov@anu.edu.au

CONTENTS

S1. EXPERIMENTAL CHARACTERIZATION OF THE METASURFACE POLARIZATION TRANSFER MATRIX

We use the experimental scheme presented in Fig. 2(d) of the main manuscript to characterize the metasurface transfer matrix. The power-meter readings are recorded over varying input states (θ_{in}) and the angle of the QWP (θ_Q), which are related to the metasurface transfer matrix $\mathbf{T}$ as follows:

$$P_{\mathrm{Det_A}} = |\langle\theta_{\mathrm{Pol_2}}|\mathbf{Q}(\theta_Q)\mathbf{T}|\theta_{in}\rangle|^2 P_{\mathrm{Det_B}}, \tag{S1}$$

where $\theta_{\mathrm{Pol_2}}$ is the orientation angle of the linear polarizer ($\mathrm{Pol_2}$), $|\theta_{in}\rangle$ is the input linear polarization state at an angle of θ_{in} selected by a corresponding rotation of HWP, $\mathbf{Q}(\theta_Q)$ is the transmission matrix of the quarter-waveplate rotated at an angle θ_Q, and $P_{\mathrm{Det_{A,B}}}$ are the measured powers at the detectors A and B. Readings were recorded over varying input states (θ_{in}) and the angle of the QWP (θ_Q). We perform numerical fitting to reconstruct from the power measurements the transfer matrix $\mathbf{T}$, up to a global phase.

Here, we prove that this procedure enables accurate and unique reconstruction of the transfer matrix. Let us first consider an idealized situation in the absence of noise. Then, according to Eq. (S1), the detected power dependence on the input polarization and QWP angles can be represented through the Fourier decomposition as

$$\begin{aligned} P_{\mathrm{r}}(\theta_{in},\theta_Q;\mathbf{T}) = P_{\mathrm{Det_A}}/P_{\mathrm{Det_B}} = \sum_{p=0,\pm2}\ \sum_{q=0,\pm2,\pm4} \Big[& \widetilde{P}_{c,c}(p,q)\cos(p\theta_{in})\cos(q\theta_Q) \\ & + \widetilde{P}_{c,s}(p,q)\cos(p\theta_{in})\sin(q\theta_Q) + \widetilde{P}_{s,c}(p,q)\sin(p\theta_{in})\cos(q\theta_Q) \\ & + \widetilde{P}_{s,s}(p,q)\sin(p\theta_{in})\sin(q\theta_Q)\Big]. \end{aligned} \tag{S2}$$

To be specific, we consider the last polarizer angle to be fixed at $\theta_{\mathrm{Pol}_2} = 0$. We find that the measured angular Fourier components can be used to reconstruct the absolute values of the transfer matrix elements as follows:

$$|T_{1,1}|^2 = [\widetilde{P}_{c,c}(0,0) + \widetilde{P}_{c,c}(2,0)] + [\widetilde{P}_{c,c}(0,4) + \widetilde{P}_{c,c}(2,4)], \tag{S3}$$

$$|T_{2,1}|^2 = [\widetilde{P}_{c,c}(0,0) + \widetilde{P}_{c,c}(2,0)] - 3\,[\widetilde{P}_{c,c}(0,4) + \widetilde{P}_{c,c}(2,4)], \tag{S4}$$

$$|T_{1,2}|^2 = [\widetilde{P}_{c,c}(0,0) - \widetilde{P}_{c,c}(2,0)] + [\widetilde{P}_{c,c}(0,4) - \widetilde{P}_{c,c}(2,4)], \tag{S5}$$

$$|T_{2,2}|^2 = [\widetilde{P}_{c,c}(0,0) - \widetilde{P}_{c,c}(2,0)] - 3\,[\widetilde{P}_{c,c}(0,4) - \widetilde{P}_{c,c}(2,4)]. \tag{S6}$$

Then, the phases can be found from the following relations, up to a global phase:

$$T_{2,1}T_{1,1}^* = [i\,\widetilde{P}_{c,s}(0,2) + 2\,\widetilde{P}_{c,s}(0,4)) + [i\,\widetilde{P}_{c,s}(2,2) + 2\,\widetilde{P}_{c,s}(2,4)], \tag{S7}$$

$$T_{2,2}T_{1,2}^* = [i\,\widetilde{P}_{c,s}(0,2) + 2\,\widetilde{P}_{c,s}(0,4)) - [i\,\widetilde{P}_{c,s}(2,2) + 2\,\widetilde{P}_{c,s}(2,4)], \tag{S8}$$

$$\mathrm{Re}(T_{1,2}T_{1,1}^*) = \widetilde{P}_{s,c}(2,0) + \widetilde{P}_{s,c}(2,4) \tag{S9}$$

$$\mathrm{Re}(T_{2,2}T_{2,1}^*) = \widetilde{P}_{s,c}(2,0) - 3\,\widetilde{P}_{s,c}(2,4) \tag{S10}$$

$$T_{2,2}T_{1,1}^* + T_{2,1}T_{1,2}^* = i\,\widetilde{P}_{s,s}(2,2) + 2\,\widetilde{P}_{s,s}(2,4). \tag{S11}$$

This analysis establishes the possibility to reconstruct both the amplitude and phase of the transfer matrix elements. However, there can be an ambiguity in determining the phase for a specific case of $T_{2,2}T_{1,1} = T_{2,1}T_{1,2}$ as then the equations are invariant to a simultaneous change of sign in solutions $\arg T_{1,2} = \arg T_{1,1} \pm \rho$, and $\arg T_{2,2} = \arg T_{2,1} \pm \rho$, where ρ is determined from Eq. (S9). Importantly, since we operate at normal incidence, the chiral effects are weak and the transfer matrix is close to symmetric, such that $T_{2,1} \simeq T_{1,2}$, and the latter condition makes the reconstruction unique by removing the phase ambiguity.

In practice, the reconstruction based on experimental data is performed by finding the transfer matrix elements that provide the best fit between the measured powers at the specific waveplate orientations and the expression according to Eq. (S1). The accuracy of reconstruction was monitored by checking the mismatch of the least means squares fitting,

$$\delta P^{(\mathrm{fit})}(\mathbf{T}) = \frac{\sum_i^N \left(P_r^{(\mathrm{fit})}(\theta_{in}^{(i)}, \theta_Q^{(i)}; \mathbf{T}) - P_r(\theta_{in}^{(i)}, \theta_Q^{(i)})\right)^2}{\sum_i^N \left(P_r(\theta_{in}^{(i)}, \theta_Q^{(i)})\right)^2}, \tag{S12}$$

where N is the total number of measurements, $\theta_{in}^{(i)}$ and $\theta_Q^{(i)}$ are the angles at the i-th measurement, and $P_r^{(\mathrm{fit})}$ is the predicted transmission ratio from Eq. (S1). This fitting was found to have

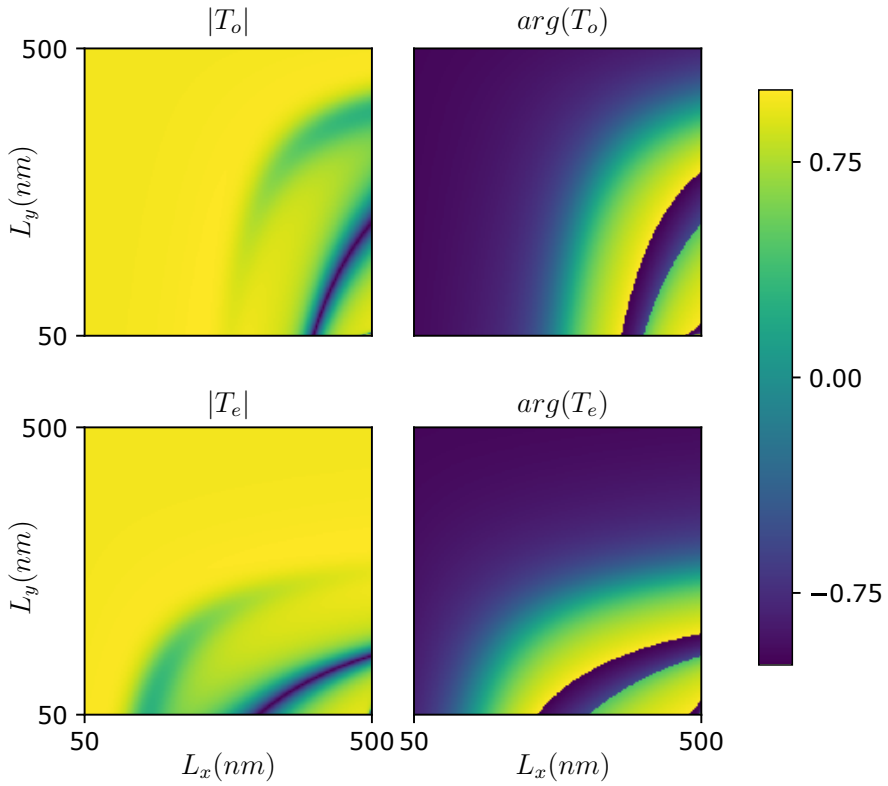

Figure S1. Numerical simulation of transfer matrix of cuboidal resonators. Shown here are the amplitudes of transmitted light in the ordinary and extraordinary axes against the physical sizes of the pixels (L_x, L_y).

mean squared error of 2.0×10^{-3} and 3.1×10^{-3} for the results shown in Figs. 3(b,c) and 4(c,d), respectively. The average mean squared error is 4.9×10^{-3} across the wavelengths for Fig. 3(e).

S2. NUMERICAL OPTIMIZATION OF THE METASURFACE DESIGN

Using Rigorous Coupled Wave Analysis (RCWA) [S1, S2], sweeps across the physical sizes of individual, cuboidal resonators without rotation were generated, see Fig. S1. These sweeps were generated using idealized refractive indices of amorphous silicon on glass. Physical parameters were then chosen from these sweeps, also accounting for a design freedom of the nanoresonator rotation. Pairwise resonators were then arranged in a metasurface according to the form of Eq. (1) for a target transfer matrix, and this analytical design was subsequently simulated numerically using a commercial electrodynamic solver, CST Studio. A notable limitation of Eq. (1) is that it does not consider near-field interactions between nanoresonators. The full simulations revealed

that these relatively weak higher order interactions do exist for some configurations. To effectively compensate for such effects, we used the CST Studio to perform optimization passes starting from an analytical design based on Eq. (1) and fine-tune the parameters to minimize the phase-invariant fidelity measure $\delta = 1 - \left|\sum_{i,j} T_{ij}^{*} \widetilde{T}_{ij}\right|^{2} \left[\sum_{i,j} T_{ij}^{*} T_{ij} \sum_{i,j} \widetilde{T}_{ij}^{*} \widetilde{T}_{ij}\right]^{-1}$, where T_{ij} and $\widetilde{T}_{ij}$ are the elements of the target and the numerically calculated transfer matrices, respectively. While this optimization step is insensitive to overall efficiency, only fine variations of the nanoresonator parameters were allowed, preserving the high efficiency of the initial design obtained from the single resonator combination design step and subsequently to CST Studio.

S3. TRANSMISSION EFFICIENCY FOR POLARIZATION PAIRS

In the manuscript, we show that by designing a metasurface with the transfer matrix according to Eq. (2), one can transform two arbitrarily chosen input polarization states $\{A_i, B_i\}$ to other two arbitrarily chosen output states $\{A_t, B_t\}$. Here we discuss the transmission efficiency of such a transformation.

Consider two arbitrary input states $A_i = \begin{bmatrix} \cos\alpha_i \\ \sin\alpha_i\, e^{i\varphi_i} \end{bmatrix}$ and $B_i = \begin{bmatrix} \cos\beta_i \\ \sin\beta_i\, e^{i\delta_i} \end{bmatrix}$, and two arbitrary output states $A_t = \begin{bmatrix} \cos\alpha_t \\ \sin\alpha_t\, e^{i\varphi_t} \end{bmatrix}$ and $B_t = \begin{bmatrix} \cos\beta_t \\ \sin\beta_t\, e^{i\delta_t} \end{bmatrix}$. The orthogonal states of the two input states are $A_i^{\perp} = i\varsigma_2 A_i^{*} = \begin{bmatrix} \sin\alpha_i\, e^{-i\varphi_i} \\ -\cos\alpha_i \end{bmatrix}$ and $B_i^{\perp} = i\varsigma_2 B_i^{*} = \begin{bmatrix} \sin\beta_i\, e^{-i\delta_i} \\ -\cos\beta_i \end{bmatrix}$ where $\varsigma_2 = \begin{bmatrix} 0 & -i \\ i & 0 \end{bmatrix}$ is the second Pauli matrix. The designed transfer matrix in Eq. (2) of the manuscript is

$$\mathbf{T}_0 = \langle A_t^{*}|B_i\rangle \cdot |B_t\rangle\langle A_i^{\perp}| - \langle B_t^{*}|A_i\rangle \cdot |A_t\rangle\langle B_i^{\perp}| = \begin{bmatrix} \tau_{11} & \tau_{12} \\ \tau_{21} & \tau_{22} \end{bmatrix}, \tag{S13}$$

where

$$\begin{aligned} \tau_{11} =& \sin\alpha_i \cos\beta_i \cos\alpha_t \cos\beta_t\, e^{i\varphi_i} + \sin\alpha_i \sin\beta_i \sin\alpha_t \cos\beta_t\, e^{i(\varphi_i+\delta_i+\varphi_t)} \\ & - \cos\alpha_i \sin\beta_i \cos\alpha_t \cos\beta_t\, e^{i\delta_i} - \sin\alpha_i \sin\beta_i \cos\alpha_t \sin\beta_t\, e^{i(\varphi_i+\delta_i+\delta_t)}, \end{aligned} \tag{S14}$$

$$\tau_{12} = \tau_{21} = \sin\alpha_i \cos\beta_i\ \cos\alpha_t \sin\beta_t\, e^{i(\varphi_i+\delta_t)} - \cos\alpha_i \sin\beta_i \sin\alpha_t\ \cos\beta_t\, e^{i(\varphi_t+\delta_i)}, \tag{S15}$$

$$\begin{aligned}\tau_{22} =&\cos\alpha_i\cos\beta_i\sin\alpha_t\cos\beta_t\,e^{i\varphi_t}+\sin\alpha_i\cos\beta_i\sin\alpha_t\sin\beta_t\,e^{i(\varphi_i+\varphi_t+\delta_t)}\\&-\cos\alpha_i\cos\beta_i\cos\alpha_t\sin\beta_t\,e^{i\delta_t}-\cos\alpha_i\sin\beta_i\sin\alpha_t\sin\beta_t\,e^{i(\delta_i+\varphi_t+\delta_t)}.\end{aligned}\tag{S16}$$

The two singular values of $\mathbf{T}_0$ are given by

$$\sigma_{\min/\max}=\frac{1}{\sqrt{2}}\sqrt{|\tau_{11}|^2+2|\tau_{12}|^2+|\tau_{22}|^2\pm\gamma}\,,\tag{S17}$$

where

$$\gamma=\sqrt{\left(|\tau_{11}|^2-|\tau_{22}|^2\right)^2+4|\tau_{12}|^2\left(|\tau_{11}|^2+|\tau_{22}|^2\right)+8\,\mathrm{Re}\left(\tau_{11}^*\tau_{12}^2\tau_{22}^*\right)}\,.\tag{S18}$$

The final transfer matrix is

$$\mathbf{T}=\frac{e^{i\phi_g}}{\sigma_{\max}}\begin{bmatrix}\tau_{11}&\tau_{12}\\\tau_{21}&\tau_{22}\end{bmatrix}=\begin{bmatrix}T_{11}&T_{12}\\T_{21}&T_{22}\end{bmatrix},\tag{S19}$$

where ϕ_g is an arbitrary global phase. For an input state A_i, the output is a pure state, $\mathbf{T}\,|A_i\rangle = t_A|A_t\rangle$, with a transmission coefficient

$$\begin{aligned}t_A&=-\frac{e^{i\phi_g}\langle B_t^*|A_i\rangle\langle B_i^\perp|A_i\rangle}{\sigma_{\max}}\\&=-\frac{e^{i\phi_g}\left(\cos\alpha_i\cos\beta_t+\sin\alpha_i\sin\beta_t\,e^{i(\varphi_i+\delta_t)}\right)\left(\sin\alpha_i\cos\beta_i\,e^{i\varphi_i}-\cos\alpha_i\sin\beta_i\,e^{i\delta_i}\right)}{\sigma_{\max}}.\end{aligned}\tag{S20}$$

When the input state is B_i, the output pure state is $\mathbf{T}|B_i\rangle = t_B|B_t\rangle$, where the transmission coefficient is

$$\begin{aligned}t_B&=\frac{e^{i\phi_g}\langle A_t^*|B_i\rangle\langle A_i^\perp|B_i\rangle}{\sigma_{\max}}\\&=\frac{e^{i\phi_g}\left(\cos\beta_i\cos\alpha_t+\sin\beta_i\sin\alpha_t\,e^{i(\delta_i+\varphi_t)}\right)\left(\sin\alpha_i\cos\beta_i\,e^{i\varphi_i}-\cos\alpha_i\sin\beta_i\,e^{i\delta_i}\right)}{\sigma_{\max}}.\end{aligned}\tag{S21}$$

Therefore, the power transmission efficiencies $T_A = |t_A|^2$ and $T_B = |t_B|^2$ depend on the inner products of the states, which relate to the distances between the states on the Poincaré sphere. Apparently, both T_A and T_B are zero when $A_i = B_i$ and $A_t \neq B_t$ because it is impossible to transform one state into two different states simultaneously. When A_i is orthogonal to the conjugate state of B_t, T_A will be zero. When B_i is orthogonal to the conjugate state of A_t, T_B will be zero. These features are evident in Fig. S2 showing the calculated transmission efficiency when four states are all linearly polarized, i.e. $\varphi_i = \delta_i = \varphi_t = \delta_t = 0$. One can see that T_A = 0 when $|\beta_t - \alpha_i| = \pi/2$ and T_B = 0 when $|\alpha_t - \beta_i| = \pi/2$. However, there are always some cases that T_A and T_B can reach 100% simultaneously.

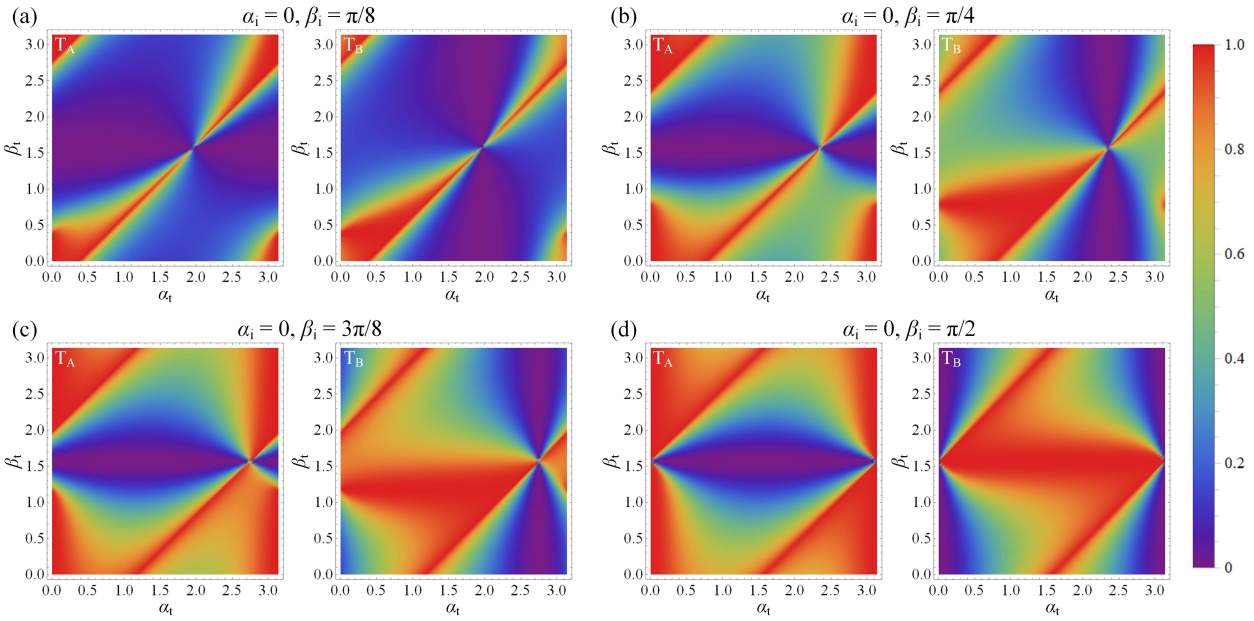

Figure S2. Transmission efficiency of the designed transfer matrix for transforming two linear polarization states into other two polarization states as functions of α_t and β_t when (a) $\alpha_i = 0$, $\beta_i = \pi/8$; (b) $\alpha_i = 0$, $\beta_i = \pi/4$; (c) $\alpha_i = 0$, $\beta_i = 3\pi/8$; and (d) $\alpha_i = 0$, $\beta_i = \pi/2$.

In general, once the two polarization pairs are chosen, the transmission efficiencies are determined based on this scheme. Once again, we highlight here that the analytical solution formulated in our work provides the best possible efficiency for a symmetric non-amplified transfer matrix, since the maximum singular value is one.

We note that a higher efficiency could be potentially achieved for some states by expanding a range of transformations to include asymmetric matrices, which would require a design of metasurfaces with a chiral response [S3]. While we consider in this work the experimental realizations of non-chiral metasurface response at normal incidence, our general analytical framework can guide future developments of complex-birefringent metasurfaces with tailored chiral response at off-normal incidence.

S4. COMPENSATION OF FABRICATION ERRORS

During the fabrication, the dimensions of the fabricated structures may be different from the designed values due to variations of the fabrication conditions in the electron beam lithography and etching. In order to compensate for the possible fabrication errors, for a single design we patterned

the same dimension multiple times using different doses during the electron beam lithography and chose the best one for the experiment. By doing so, the transfer matrix of the best structure appeared to be very close to the designed one. The slight difference can result in a position shift of A_t and B_t with respect to the designed places on the Poincaré sphere and a small variation of the transmission efficiency. However, we emphasize that once the sample is characterized, its transfer matrix is determined with high precision and thus the output polarization state for a specific input state is also well defined. Therefore, any small fabrication errors are fully taken into account in our experiment and data analysis.

S5. TRANSFORMATION OF ELLIPTICAL POLARIZATION STATES

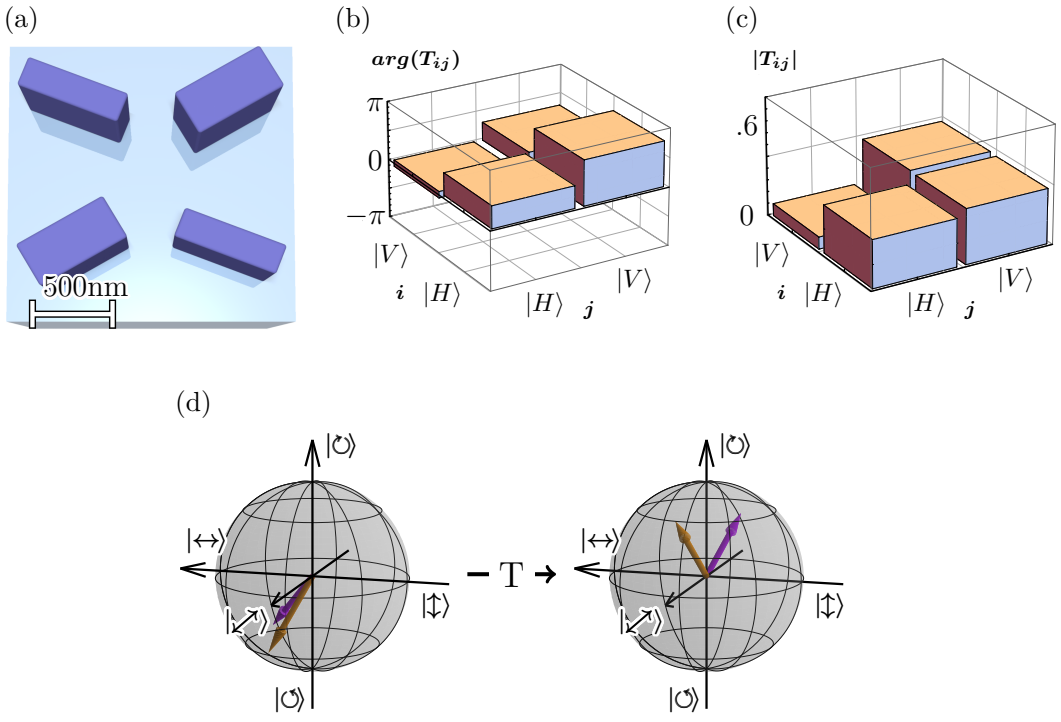

Figure S3. Metasurface design for the transformation of a pair of two elliptical polarization states to the other chosen states. (a) Three-dimensional render of the metasurface. (b, c) The numerically simulated (b) arguments and (c) absolute values of the transfer matrix at a wavelength of $1550nm$. (d) The transformation of states calculated from the numerical model.

Under our scheme, it is possible to transform between arbitrary input to output pairs of polar-

ization states, including any elliptical ones. As an illustration, we show in Fig. S3 the application of the general approach to the following pairs of input states,

$$|A_i\rangle = \begin{bmatrix} \cos(30.0^\circ) \\ \sin(30.0^\circ)e^{-i\,0.5\pi} \end{bmatrix}, \quad |B_i\rangle = \begin{bmatrix} \cos(27.5^\circ) \\ \sin(27.5^\circ)e^{-i\,0.7\pi} \end{bmatrix}$$

and the target output states

$$|A_t\rangle = \begin{bmatrix} \cos(41.6^\circ) \\ \sin(41.6^\circ)e^{i\,0.25\pi} \end{bmatrix}, \quad |B_t\rangle = \begin{bmatrix} \cos(49.0^\circ) \\ \sin(49.0^\circ)e^{i\,0.82\pi} \end{bmatrix}$$

We designed and numerically optimized a metasurface, which achieves the transmission efficiencies $T_A = 43.2\%$ and $T_B = 28.2\%$. The numerically determined transfer matrix has singular values of $\sigma_{\max} = 0.91$ and $\sigma_{\min} = 0.18$, demonstrating that the design is close to optimal as the largest singular value is close to one.

References

(S1) P. Lalanne, Improved formulation of the coupled-wave method for two-dimensional gratings, J. Opt. Soc. Am. A **14**, 1592 (1997).

(S2) P. Lalanne and G. M. Morris, Highly improved convergence of the coupled-wave method for tm polarization, J. Opt. Soc. Am. A **13**, 779 (1996).

(S3) Z. Shi, A. Y. Zhu, Z. Li, Y.-W. Huang, W. T. Chen, C.-W. Qiu, and F. Capasso, Continuous angle-tunable birefringence with freeform metasurfaces for arbitrary polarization conversion, Sci. Adv. **6**, eaba3367 (2020).